Received: January 30, 2019 Revised: June 21, 2019 Accepted: June 26, 2019

(onlinelibrary.wiley.com) DOI: 10.1111/ner.13025

Design and Evaluation of a Rodent-Specific Transcranial Magnetic Stimulation Coil: An *In Silico* and *In Vivo* Validation Study

Julia Boonzaier, MSc*; Petar I. Petrov, MSc†; Willem M. Otte, PhD*‡; Nickolay Smirnov, PhD§; Sebastiaan F.W. Neggers, PhD†; Rick M. Dijkhuizen, PhD*

Background: Rodent models are fundamental in unraveling cellular and molecular mechanisms of transcranial magnetic stimulation (TMS)-induced effects on the brain. However, proper translation of human TMS protocols to animal models have been restricted by the lack of rodent-specific focal TMS coils.

Objective: We aimed to improve TMS focalization in rodent brain with a novel small, cooled, and rodent-specific TMS coil.

Methods: A rodent-specific 25-mm figure-of-eight TMS coil was developed. Stimulation focalization was simulated *in silico* for the rodent coil and a commercial human 50-mm figure-of-eight TMS coil. Both coils were also compared *in vivo* by electromyography measurements of brachialis motor evoked potential (MEP) responses to TMS at different brain sites in anesthetized rats (n = 6). Focalization was determined from the coils' level of stimulation laterality. Differences in MEPs were statistically analyzed with repeated-measures, within-subjects, ANOVA.

Results: *In silico* simulation results deemed the human coil insufficient for unilateral stimulation of the rat motor cortex, whereas lateralized electrical field induction was projected attainable with the rodent coil. Cortical, *in vivo* MEP amplitude measurements from multiple points in each hemisphere, revealed unilateral activation of the contralateral brachialis muscle, in absence of ipsilateral brachialis activation, with both coils.

Conclusion: Computer simulations motivated the design of a smaller rodent-specific TMS coil, but came short in explaining the capability of a larger commercial human coil to induce unilateral MEPs *in vivo*. Lateralized TMS, as demonstrated for both TMS coils, corroborates their use in translational rodent studies, to elucidate mechanisms of action of therapeutic TMS protocols.

Keywords: Electric fields, finite element analysis, motor evoked potential, rats, transcranial magnetic stimulation

Conflict of Interest: The commercial roles of Nickolay Smirnov and Sebastiaan F. W. Neggers did at no point influence the design, the execution of experiments, data analysis or conclusions in the present manuscript. Nickolay Smirnov is chief commercial officer at Neurosoft, Ivanovo, Russia. Neurosoft manufactures and markets the rat TMS coil that was used and tested for the first time in the current manuscript. Besides his role as associate professor at the UMC Utrecht, De Bilt, The Netherlands, Sebastiaan F. W. Neggers is one of the founders of and has shares in Brain Science Tools BV and act as its managing CEO. Brain Science Tools BV is currently a Neurosoft distributor for the Netherlands. The remaining authors have no conflicts of interest to report.

Address correspondence to: Rick M. Dijkhuizen, Biomedical Magnetic Resonance Imaging and Spectroscopy Group, Center for Image Sciences, University Medical Center Utrecht, Yalelaan 2, 3584 CM Utrecht, The Netherlands. Email: r.m.dijkhuizen@umcutrecht.nl

* Biomedical Magnetic Resonance Imaging and Spectroscopy Group, Center for Image Sciences, University Medical Center Utrecht and Utrecht University, Utrecht, The Netherlands;
† Department of Psychiatry, Brain Center Rudolf Magnus, University Medical Center Utrecht and Utrecht University, Utrecht, The Netherlands;
‡ Department of Pediatric Neurology, Brain Center Rudolf Magnus, University Medical Center Utrecht and Utrecht University, Utrecht, The Netherlands; and
§ R&D Department, Neurosoft, Ivanovo, Russia

For more information on author guidelines, an explanation of our peer review process, and conflict of interest informed consent policies, please go to http://www.wiley.com/WileyCDA/Section/id-301854.html

Source(s) of financial support: This work was funded by the Netherlands Organization for Scientific Research [VICI 016.130.662] and by the DeNeCor project being part of the ENIAC Joint Undertaking.

INTRODUCTION

Transcranial magnetic stimulation (TMS) is a noninvasive brain stimulation technique that has been widely used to modulate cortical excitability and to study central nervous system physiology in healthy subjects and patients (1). Repetitive TMS (rTMS) protocols have shown therapeutic potential in several neurological and psychiatric disorders (2), however, the cellular and molecular mechanisms underlying TMS-induced neurorecovery remain poorly understood (3). These mechanisms could be systematically studied in rodent models; however, there is a lack of rodent-specific TMS coils (4).

TMS studies in rodents have regularly made use of commercial human coils (5). Due to their relatively large size, these coils induce a broad volume of electrical current, resulting in widespread stimulation of the small rodent brain (3,5), which limits the translational relevance to human TMS applications (5). Nevertheless, Rotenberg and colleagues have shown that a commercial human TMS coil can be used to reliably generate unilateral motor evoked potentials (MEPs) from the forelimb of the rat (6). The authors accomplished this by laterally positioning the coil over a rat brain hemisphere. This coil position only allows a fraction of the electromagnetic field to be applied to a single hemisphere, resulting in focal stimulation and unilateral MEPs.

Although smaller rodent-specific TMS coils could theoretically improve focalization of brain stimulation, development of miniature TMS coils has been challenging due to increased resistance, overheating, and coil rupture (7). Parthoens and colleagues have shown that coil size can be significantly reduced, however, they were unable to demonstrate improved focalization, evidenced by the lack of MEP laterality during motor threshold (MT) determination (8). Other studies have shown that rodent-specific coils with reduced stimulation intensity have greater focality (4,9,10). However, the effects induced by these low-intensity stimulation coils, may not be representative of the changes induced by high-intensity stimulation coils as used in human TMS studies (11). Furthermore, a recent study by Meng and colleagues has proposed the design of a figure-0 shaped coil with a ferromagnetic core (12). This design requires less power to achieve similar magnitudes of the induced electric field as compared to the more common no-core coil designs. The authors demonstrated a novel mechanism to shift the induced magnetic field and thus create more focal stimulation than traditionally possible with such circular shaped coil designs. Although this coil improves focality, its composition with tightly packed coil wirings will unlikely withstand more demanding rTMS protocols. Consequently, there is a need for small animal coils that can deliver TMS and rTMS at intensities similar to human studies, while maintaining a good degree of focality. This could facilitate studies in animal models of disease to develop, test, and guide TMS-based therapies for clinical use (5).

Therefore, in this study we first modeled the stimulation focality of a commercial human figure-of-eight coil (50 mm), by employing the finite element modeling method (FEM) in electro-magnetic computer simulations to a 3D anatomical magnetic resonance imaging (MRI) dataset of the rat brain. Based on these *in silico* simulation results, we developed a small, rodent-specific figure-of-eight coil (25 mm). Subsequently, we tested whether these coils could focally stimulate the rat primary motor cortex through *in silico* simulation of the field profiles and *in vivo* measurement of brachialis MEP responses in the rat. We hypothesized that a smaller rodent coil would allow more focal stimulation of cortical rat brain tissue than a large commercial human TMS coil.

MATERIALS AND METHODS

In Silico Experiments

Computer Simulation

Computer simulations were conducted using the free open source software package SCIRun 4.7+ (A Scientific Computing Problem Solving Environment, Scientific Computing and Imaging Institute, Salt Lake City, UT, USA). Two additional modules were developed, namely one for generating the geometry of thin wire coils and another for solving their respective induced electromagnetic fields based on the Biot-Savart law (see Petrov et al. (13), https://github.com/pip010/scirun4plus).

Head Model

A 3D rat brain model, consisting of white matter-, gray matter-, and cerebrospinal fluid-labeled voxels was constructed from a high-resolution MRI template, as described in the Supporting Information (see Material and Methods, Head model). The MRI template and tissue segmentations are available for download (14).

The generation of a 3D mesh from the segmented image, 168 × 137 × 273 matrix size and 94 μm resolution, was done with the Cleaver 2, a free multi-material tetrahedral meshing tool developed by the NIH Center for Integrative Biomedical Computing at the University of Utah's Scientific Computing and Imaging (SCI) Institute (https://github.com/SCIInstitute/Cleaver2/releases) (15).

We generated an adaptive mesh using the following input parameters: sizing field 2.0, sampling resolution 1.0, and Lipschitz/grading 3.0. Preprocessing was applied to the initial binary segmentation where each compartment was isolated and iteratively smoothed via multiple steps of inflate-deflate (smooth parameter = 0.5, see BioMesh3D [part of SCIRun4 https://www.sci.utah.edu/cibc-software/scirun/biomesh3d.html, step 1 and 2 only]). The procedure resulted in a mesh with 628,897 nodes and 3,551,606 elements. The following isotropic conductivity properties were set for each relevant tissue compartment: gray matter 0.33 S/m (8); white matter 0.25 S/m, estimated as an average of its 1:3 ratio of 0.125 S/m (16); CSF 1.7 S/m. These values are similar to human conductivities at low frequency <10 kHz. No anisotropic properties were captured, which were relevant for the white matter only.

We modeled the white matter with homogeneous electrical conductivity. Taking white matter anisotropy into account in FEM equations mainly has the effect of more current accumulation along white matter tracts (17). As these induced electric fields estimated by FEM are generally only a small percentage of the total currents that are dominated by the incident electric field from the TMS coil, this can be expected to have little effect on the difference between total currents evoked by TMS in the right and left hemispheres of the rat brain. The rat cortex does not at all show gyrification like the human brain. Thus, it is expected that taking into account white matter anisotropy will only lead to somewhat stronger current estimates below the gray matter sheet. What such deeper induced fields signify and if and how they lead to actual action potential generation along white matter tracts is completely unknown as of yet, and highly speculative. We assessed induced currents in the gray matter only, which, also according to Opitz and colleagues (17), is hardly affected by taking into account white matter anisotropy, further justifying our approach.

Coil Models

Two figure-of-eight coil models were constructed (Fig. 1), namely one coil with a diameter of 50 mm (equivalent to a readily available commercial human coil by Neurosoft, Ltd., Ivanovo, Russia), and a second coil with a 25 mm diameter. Initial simulation results suggested that induced currents from the 25 mm coil were mainly focalized unilaterally. Therefore, we requested Neurosoft to manufacture this coil. Due to its small size, and our ambition to use this coil for rTMS studies, the coil also had to be equipped with cooling which was achieved with silicone oil. To maintain efficient cooling, the design of the smaller coil was based on a sparser wire distribution

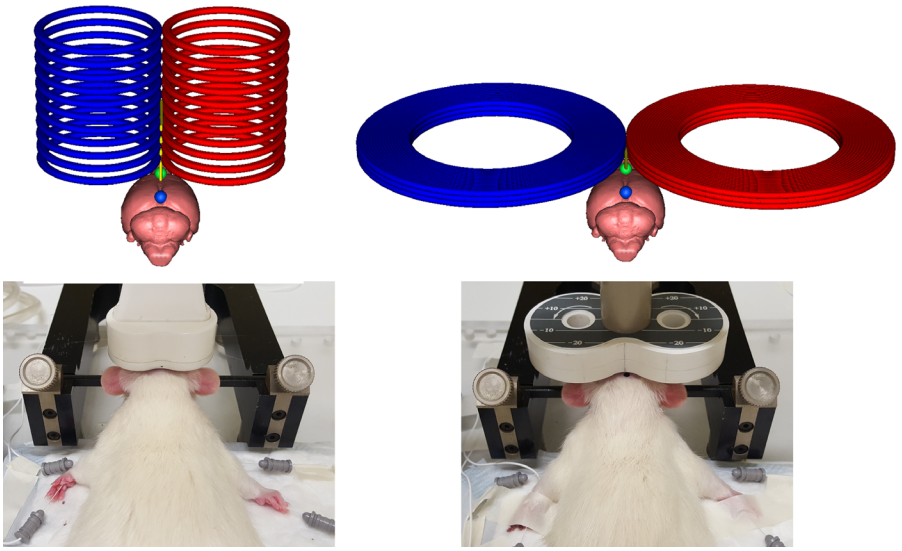

Figure 1. Overview of the finite element modeling (FEM) simulation and experimental coil setup. In the top and bottom rows, the simulation and experimental setup of coil orientation and positioning are demonstrated for the small (left) and large (right) TMS coils, respectively. In the top row, the coil is positioned along the mid-line of the brain over bregma (green sphere) at a fixed (~1 cm) offset from a second anatomical landmark (blue sphere), which is located at the interaural line. In the bottom row, we illustrate that the *in vivo* coil setup matches that of the simulation experiments. In these images, bregma is not visible, but the posterior end of the coil is positioned on the interaural landmark, which was used as a starting reference location when positioning the coil during active experiments. From this position, the coil was moved anterolaterally to position the center of each coil over the forelimb region of the motor cortex. TMS, transcranial magnetic stimulation. [Color figure can be viewed at wileyonlinelibrary.com]

(winding) compared to the larger uncooled coil. This resulted in coil heights of 24 and 18.5 mm for the small and large coil, respectively. The differences in the coil heights would not lead to any significant changes in the simulation results. The current is equally distributed among each layer of the coils and it has a small effect on the depth/penetration of the field.

The geometric generation of the coils were implemented in additional modules to SCIRun 4.7 (Table 1 for coil parameters) (13). The same procedure, as explained by Petrov and colleagues, was used to derive the peak current driven through the coil for the bi-phasic Neurosoft TMS (13). This resulted in current values of 6.4×10^6 A/s (80% MO) for the small coil and 3.6×10^6 A/s (45% MO) for the large coil.

Cortical Region of Interest

We constructed a small region of interest (ROI) patch in the form of a lattice 3D mesh ($16 \times 17 \times 2$ voxels, $8 \times 8.5 \times 1$ mm^3 size, resolution 0.5 mm), which was placed superficially (~1 mm depth) on each hemisphere of the rat cortex in the mesh obtained from the segmented image. The area corresponding to the forelimb region of the rat's primary motor cortex was masked in accordance with the mapping study of Fonoff et al. (18). Their study provides an accurate (0.5 mm resolution grid, same as our ROI) functional map of the primary motor cortex in relation to bregma, determined from microelectrodes and electromyography (EMG) MEPs.

To place each ROI patch in our model, we defined lambda in relation to the interaural line, from which bregma was allocated at 8.34 mm anterior to lambda. The patch was visually aligned, in orthogonal view, with the outer/superior gray matter surface. The distance of 8.34 mm was derived from the linear regression formula, $Y = bX + a$ (Y = distance of the interaural line to bregma, X = rat weight, a and b are constants) as suggested by Whishaw et al. (19), and the average body weight of the MRI-scanned rats. Considering this formula, the discrepancy with our experimental rat population (average weight: 413 g) was found to be around 5.5% (<0.5 mm), hence we attempted no compensation in modeling.

In this study, the ROI was used to assess a value from modeled currents by accumulating the current over the ROI. This value is hypothesized to scale with MEPs as this region projects down the corticospinal tracts. Details of the neuromuscular system nor the EMG needle electrodes used to measure MEPs were modeled. Hence this approach does not allow absolute predictions of MEP amplitudes in terms of mV, and modeled MEP amplitudes are therefore expressed in arbitrary units (AU).

Table 1. Parameters for Coil Modeling and Generation (SCIRun:: CreateTMScoil).

Coil parameters	Small coil	Large coil
Machine output (MO)	80%	45%
max|dI/dt|	6.4×10^6 A/s	3.6×10^6 A/s
Windings	2	17
Radius inner	9.5 mm	14.5 mm
Radius outer	10.5 mm	23.5 mm
Distance outer	1 mm	1 mm
Stacks	10	3
Stack step	1.5 mm	1 mm
LOD	2	2

In Vivo Experiments

Animals

Six naïve adult male Sprague Dawley rats (413 ± 21 g, mean ± standard deviation; Charles River, Sulzfeld, Germany) were used. Experiments were approved by the Animal Ethics Committee of the University Medical Center Utrecht, The Netherlands, and were conducted in agreement with Dutch laws ("Wet op de Dierproeven," 1996) and European regulations (Guideline 86/609/EEC). Animals were housed in pairs under controlled environmental conditions (12 hour-light/dark cycle, temperature 20–24°C, 45–65% humidity),

with *ad libitum* access to food and water, and with a Perspex tube as cage enrichment.

Animal Preparation and Anesthesia

Rats were briefly anesthetized with a mixture of medical oxygen and isoflurane (5% induction, 2.5% maintenance) for the placement of a lateral tail vein catheter preloaded with heparinized saline (50 U.I./mL), followed by the continuous infusion of propofol (40 ± 2 mg/kg/hour; Fresenius Kabi, The Netherlands). Propofol anesthesia was used during MEP recordings, because at low propofol doses, stable MEP responses can be measured over a period of four hours (20).

Isoflurane was maintained at 2.5% during the first 5 min of propofol infusion, where after isoflurane delivery was discontinued. A 20-min washout period of isoflurane was endorsed, before the onset of MEP measurements, to limit the suppressive effect of isoflurane on MEPs (21,22). Meanwhile, the rat's head was shaved (to ensure close contact of the TMS coil with the skull) and the animal was fixed in a stereotaxic frame. During the entire experimental procedure, the body temperature of the animals were maintained at 37°C using a rectal temperature feedback probe connected to a circulating water-heated pad system.

Electromyography

MEPs were recorded from the forelimbs of each animal with monopolar, 28G stainless steel needle electrodes (Neuroline, Ambu A/S, Ballerup, Denmark), inserted into the belly of each brachialis muscle. The location of the brachialis muscle was determined by palpation of the forelimb in the extended position. The needle electrodes were presoaked in saline (0.9% NaCl, B. Braun, Melsungen AG, Germany) before insertion, to ensure low impedance (23). After insertion, the electrodes were secured and held in place by adhesive tape. A reference electrode was positioned distally in the footpad of the forelimb. Each animal was electrically grounded with a single disposable subdermal needle electrode (Technomed Europe, The Netherlands), inserted into the base of the tail. The EMG signal was band-pass filtered between 5 and 10 kHz, and amplified by a factor of 164 in the range of up to 60 mV (Neuro-MEP-4 system, Neuro-MEP software, Version 3.4.25.0, Neurosoft, Ltd.). EMG signal was digitized with a 20 kHz sampling rate and traces were stored in XML files for further analysis using MATLAB.

Transcranial Magnetic Stimulation

All animals were stimulated with a biphasic Neuro-MS/D stimulator using a small (25 mm) and a large (50 mm) figure-of-eight TMS coil, manufactured by Neurosoft, Ltd. (see section "Coil models" above for details). During stimulation, each coil was fixed horizontally in the posterior–anterior orientation into a manipulator and secured to the stereotaxic frame (Fig. 1, bottom row). This allowed movement of the coil along three axes.

To conduct the TMS-MEP measurements in a consistent manner, the anterior–posterior coordinates of bregma were calculated relative to the interaural line, as described by Whishaw and colleagues (19). The central point of the interaural line was used as a zero reference point for positioning the center of the coil over the forelimb region of the rat's motor cortex. First, the posterior end of the coil was positioned on the zero reference point. Second, the coil was moved posteriorly to position the center of the coil over bregma. Finally, from bregma the coil was moved in the anterolateral direction to position the coil above the cortical forelimb region. The center of the forelimb region was estimated to be 1 mm anterior and 2.5–3 mm lateral to bregma based on functional mapping of the rat motor cortex (18). Small differences in coil center positioning reflected minor variances in skull width and snout curvature.

Motor Threshold Determination

The MTs for the left and right hemispheres were determined independently for each coil. Single pulses were administered to the left motor cortex, followed by stimulation of the right motor cortex, or vice versa. MEPs were recorded with Neuro-MEP software (Version 3.4.25.0, Neurosoft, Ltd.). To determine the location over the motor cortex where MEPs could be reliably measured, the coil was moved both anteroposteriorly and mediolaterally over the left and right hemispheres in steps of 1 mm. At each location, an approximation of the MT was obtained by starting stimulation at 20% (large coil) or 50% (small coil) of the maximum MO and increasing the intensity in steps of 5% until a positive MEP response was recorded. A positive MEP response was defined as a MEP with a peak-to-peak amplitude of at least 50 μV. Due to signal noise and the polymorphic nature of the MEPs we often observed MEP amplitudes of ≥0.1 mV. The estimated MT was regarded as the minimum intensity at which minimally five of ten consecutive trials resulted in positive MEPs (24). To exclude the possibility of low frequency rTMS-induced effects, we allowed a minimum of 10 sec between stimulation pulses (25,26).

Additional MEPs were recorded at four adjacent locations in each hemisphere, namely: 1 mm medial, 1 mm anterior, 1 mm lateral, and 1 mm posterior to the central location. At each location, including the central location, we stimulated at 100% of the approximated MT for each hemisphere and recorded 10 EMG traces. Similar grid measurements in humans are typically done at 110–120% of the MT, but because of the larger MEP amplitudes that we recorded (≥0.1 mV vs. 0.05 mV in humans), we used a lower stimulation intensity for these grid measurements.

Data Analysis

Each EMG trace was analyzed in MATLAB (MATLAB and Statistics Toolbox Release 2012b, The MathWorks, Inc., Natick, MA, USA). The MEP amplitude was determined from the difference between the minimum and maximum EMG reading values between 7 and 25 ms after TMS discharge. No dynamic analysis was performed to detect the time points of MEP onset and end, or the maximum and minimum amplitudes, as the shape of the MEPs were quite variable over coils and rats, and generally had a complex polyphasic morphology (27,28) (see Results section), which was less reproducible as compared to human MEPs (29).

We performed a visual inspection of all trials and verified that the automated MEP amplitude detection was accurate. In five rats, a few single recordings were excluded because of ripple-like spurious signals (see Results section). From one rat all recordings were excluded because of a high degree of spontaneous EMG activity, probably caused by anesthesia problems.

First, average MEP amplitudes for each forelimb, calculated from ten consecutive EMG traces, were determined for every stimulation location (five per hemisphere), for each coil. Next, differences in MEPs were statistically analyzed with a repeated-measures, within-subjects, ANOVA ($2 \times$ COIL TYPE, $3 \times$ LOCATION, $2 \times$ HEMISPHERE, $2 \times$ FORELIMB) using IBM SPSS statistics (version 20, IBM, Armonk, NY, USA). Values were classified as statistically significantly different if $p < 0.05$.

RESULTS

TMS Coil Laterality

In Silico Validation

To evaluate the incident electric field, namely the primary electric field produced by the coil alone, we considered a surface plane (10×10 mm^2) positioned at different offsets (z-offset) along the iso-

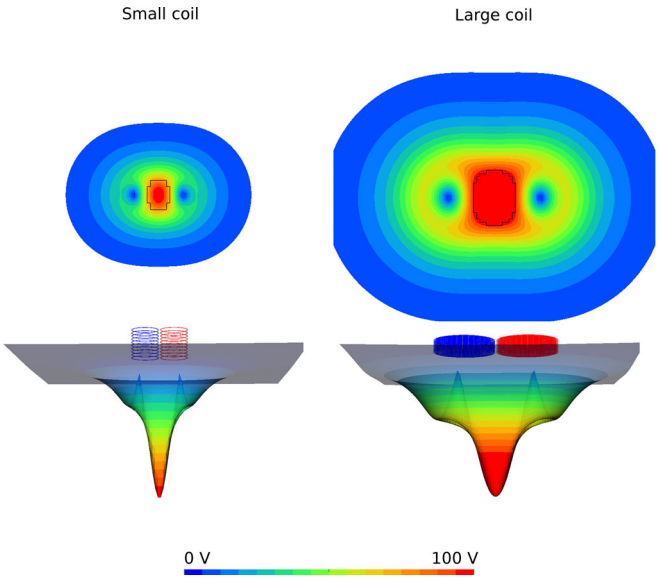

Figure 2. Simulation of the primary electric fields (coil contribution only) for the small and large coils. Top row: Rendered surfaces (top view) of the inflated surfaces (bottom row). The black line, outline (iso-line) in the rendered surfaces, depicts the extent of the half power region (HPR). Bottom row: The inflated surfaces show a *z*-axis inflated square mesh with a factor of $z = z + 0.1*|Et|/\max(|Et|)$; where Et is the final total electric field (the primary coil and secondary FEM derived electric fields combined). The distance between the surface of each coil and the square mesh is 5 mm, a relevant anatomical depth around which we expect the strongest cortical stimulation possible. [Color figure can be viewed at wileyonlinelibrary.com]

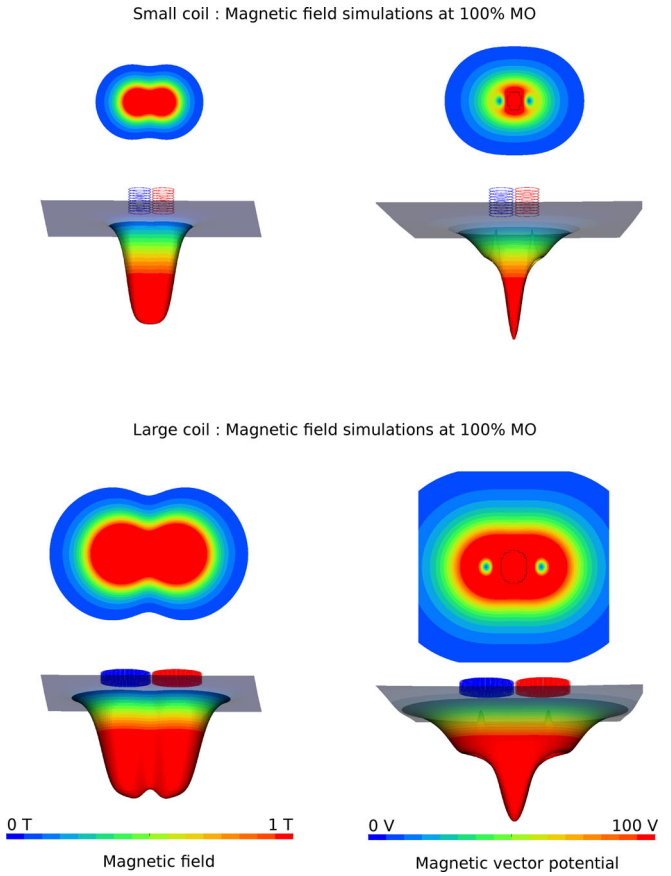

Figure 3. The simulated electrical and magnetic fields produced by the small and large TMS coils. Visualization of the magnetic field (left) and the magnetic vector potential (right) for the small and large TMS coils. The measured location is a plane positioned at 5 mm offset from the primary coil surface. Top row, for small and large coil: Field magnitude map (grid of 128 × 128 for a size of 10 × 10 mm). Bottom row, for small and large coil: 3D visualization of an artificially inflated triangular surface to depict the general shape of each field. The degree of deformation along the primary axis is proportional to the magnitude map depicted in the top row. MO, machine output. [Color figure can be viewed at wileyonlinelibrary.com]

centers of the coils. In particular we compared the fields of the small coil to that of the large coil (Fig. 2) at a depth z-offset of 5 mm below their surface, where we defined 100 V/m as a reference threshold value for successful neuronal activation (30). In Figure 2 (top row), the half power region is depicted as a measure of focality, defined as the area where the total electric field, *E*, obeys the condition $|E| > |E\_maximum = 100\ V|/sqrt\ (2)$ (30), with a small to large coil ratio of 32:60 mm^2. Although these results are indicative of better focal stimulation in favor of the small coil, it also hints at possible power impotence in comparison to the large coil, consequently having an effect on the capability of the small coil to sufficiently stimulate neuronal populations involved in eliciting MEPs. This predicament can be supported further when considering the depth decay of the fields of each coil at an individually fixed MO. The field of the large coil drops by 20% from $z = 5$ mm to $z = 10$ mm, and by 35% from $z = 10$ to 20 mm, whereas the small coil drops by 27 and 40%, respectively. In addition, using the same approach, we validated the magnetic field for each coil at a distance of 5 mm and 100% of the MO to values/plots provided by the manufacturer, as shown in Figure 3.

The simulation results (Fig. 4) were obtained with a MO of 80 and 45% for the small and large coils, respectively. These intensities were selected as the most representative MO for each coil based on our *in vivo* experiments. The computer simulations of the complete electrical field for the large coil showed similar values in ipsi- and contralateral homologous regions, despite lateralized positioning of the coil center. This was demonstrated for three different locations on each side of the cerebrum (−4, −3, −2, 2, 3, and 4 mm from midline) evaluated on the ROI patches (Fig. 4). The slight asymmetry in the electrical field between the hemispheres can be explained by the minor anatomical asymmetry of white matter in our sample of rat brain images. An integral of the electrical and current density vector fields on each side of our predefined ROI grids (see Methods section, "Cortical region of interest") is shown in relation to MEP recordings in Figure 6 (top panel) for each of the three simulated coil positions on each side (for each hemisphere).

In Vivo Validation

In vivo TMS experiments revealed that the small coil needed about double the amount of MO intensity compared to that of the large coil to generate MEPs and to determine the MTs (see Supporting Information, Results, Table S1). The average MTs for the small coil were: 73 ± 8% MO (right hemisphere) and 81 ± 4% (left hemisphere). Whereas, the average MTs for the large coil were: 42 ± 3% MO (right hemisphere) and 45 ± 4% MO (left hemisphere). For both TMS coils, the intensity of the MT varied with 0–10% between hemispheres. In one animal we observed a 25% MO intensity difference between hemispheres for the small coil.

At 100% MT, the contralateral brachialis MEP amplitude was determined from the difference between the minimum and maximum EMG reading values between 7 and 25 ms after TMS discharge (Fig. 5a,b). The MEPs generally had a complex polyphasic

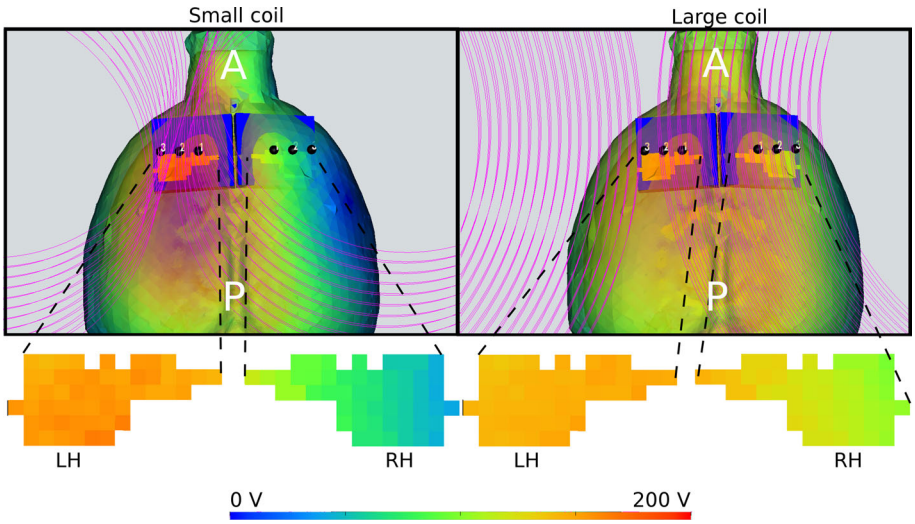

Figure 4. Simulation results for the region of interest in the brain model. Top row: Rendering of the total electric field, as a transparent overlay (10% opacity) over the outer cortex boundary of the FEM 3D model, for the small and large coils. The blue overlay on top of the brain shows the delineation of the frontlimb region of the motor cortex as the region of interest (ROI). Black spheres in this overlay, illustrate three locations in each hemisphere where coil positions were sampled. The results shown here, only refer to the coil positioned at the outer left location of the left hemisphere (LH). Bottom row: Enlarged, isolated ROI patches show the simulated electric field for each coil, within each hemisphere. LH, left hemisphere; RH, right hemisphere; A, anterior; P, posterior. [Color figure can be viewed at wileyonlinelibrary.com]

morphology with one or two prominent peaks, followed by a variable number of lower amplitude peaks. In some rats, we also observed visible ripple-like signal peaks that seemed to be unrelated to the TMS pulse (Fig. 5c,d).

Coil laterality was evaluated from averaged MEP amplitudes, recorded bilaterally from the left and right forelimbs, evoked from five stimulation positions over each hemisphere, that is, a central location of the motor cortex, and locations at 1 mm anterior, medial, posterior, and lateral of the central location, respectively (Figs. 6 and 7). The MEP amplitude maps (Fig. 7) showed that clear lateralization can be observed for both the large and the small TMS coils, different from the *in silico* results where the large coil hardly exhibited lateralization (Fig. 6). Both TMS coils occasionally induced small MEP responses in the ipsilateral forelimb, but the largest MEP responses were observed in the contralateral forelimb. Interestingly, the relative hotspot (center of motor cortex) area did not always yield the highest MEP responses.

To further validate coil laterality statistically, MEP amplitude data from three lateral stimulation positions in each hemisphere (POS = 6 stimulation positions) were plotted (Fig. 6, bottom panel). A significant interaction between TMS stimulation position and forelimb channel on MEP amplitude (POS × LIMB: [$F_{5,\ 4} = 13.965$, $p = 0.01$]), statistically confirmed the main lateralization effect (larger responses in the forelimb contralateral to the stimulated hemisphere). A significant difference was observed in MEP amplitude when considering the interaction between coil size, stimulation position, and forelimb channel (COIL × POS × LIMB: $F_{5,\ 4} = 8.212$, $p = 0.014$]). The latter seems to reflect a stronger lateralization for the large coil, which may be explained by the larger MEP amplitudes elicited by the large coil.

DISCUSSION

The aim of the present study was to evaluate the focality of a conventional figure-of-eight TMS coil (50 mm) and a rodent-specific miniaturized figure-of-eight (25 mm) TMS coil. FEM simulations predicted that the large conventional TMS coil would be unable to achieve lateralized focal stimulation of the rat motor cortex. Therefore, we hypothesized that the small rodent-specific TMS coil would more focally elicit lateralized MEPs compared to the large coil. However, unexpectedly, our *in vivo* data showed that both TMS coils were able to elicit unilateral MEPs from the contralateral forelimb of the rat.

In contrast to some recently designed rodent-specific TMS coils (4,8), our small figure-of-eight coil successfully induced focal stimulation and elicited MEPs. In rats, MEPs of similar size as in our study have been induced with a 40-mm bended circular coil, but stimulation laterality could not be achieved (8). In a recent study, Meng et al. measured unilateral MEPs (0.1–0.2 mV) in mice with a silicon steel-based 25-mm cylindrical coil, however, MT determination and MEP mapping were not reported (12). Thus, the assessment of TMS-induced MEPs and corticospinal excitability studies in rodents using appropriately sized coils remain limited. Coil size reduction is still extremely challenging because of heating and mechanical stress from electromagnetic forces, due to increased resistance and larger currents needed to produce an effective magnetic field (31). Through effective silicone oil cooling, our small figure-of-eight rodent-specific coil could deliver focal stimulation pulses at intensities similar to conventional TMS coils.

Lateralized MEPs recorded with the large TMS coil is consistent with the findings of Rotenberg and colleagues and Vahabzadeh-Hagh et al. who used similarly sized commercial TMS coils to stimulate the rat motor cortex (6,32). This was inconsistent with our *in silico* simulations, in which the incident electrical fields for the large TMS coil were only marginally different between the left and right motor cortex. We hypothesize that our simulated cortical ROI is underrepresentative of the full population of neurons that is involved in a typical rat MEP response. Due to the width and strength of the electrical field produced by the large coil (Fig. 2), it might have recruited a broader range of neuronal populations or even deeper subcortical structures (below the ~1 mm-thick skull and the ~1 mm-thick cortex) that could have influenced various descending tracts involved in the MEP response. Consequently, the focality of both the large and small TMS coils may

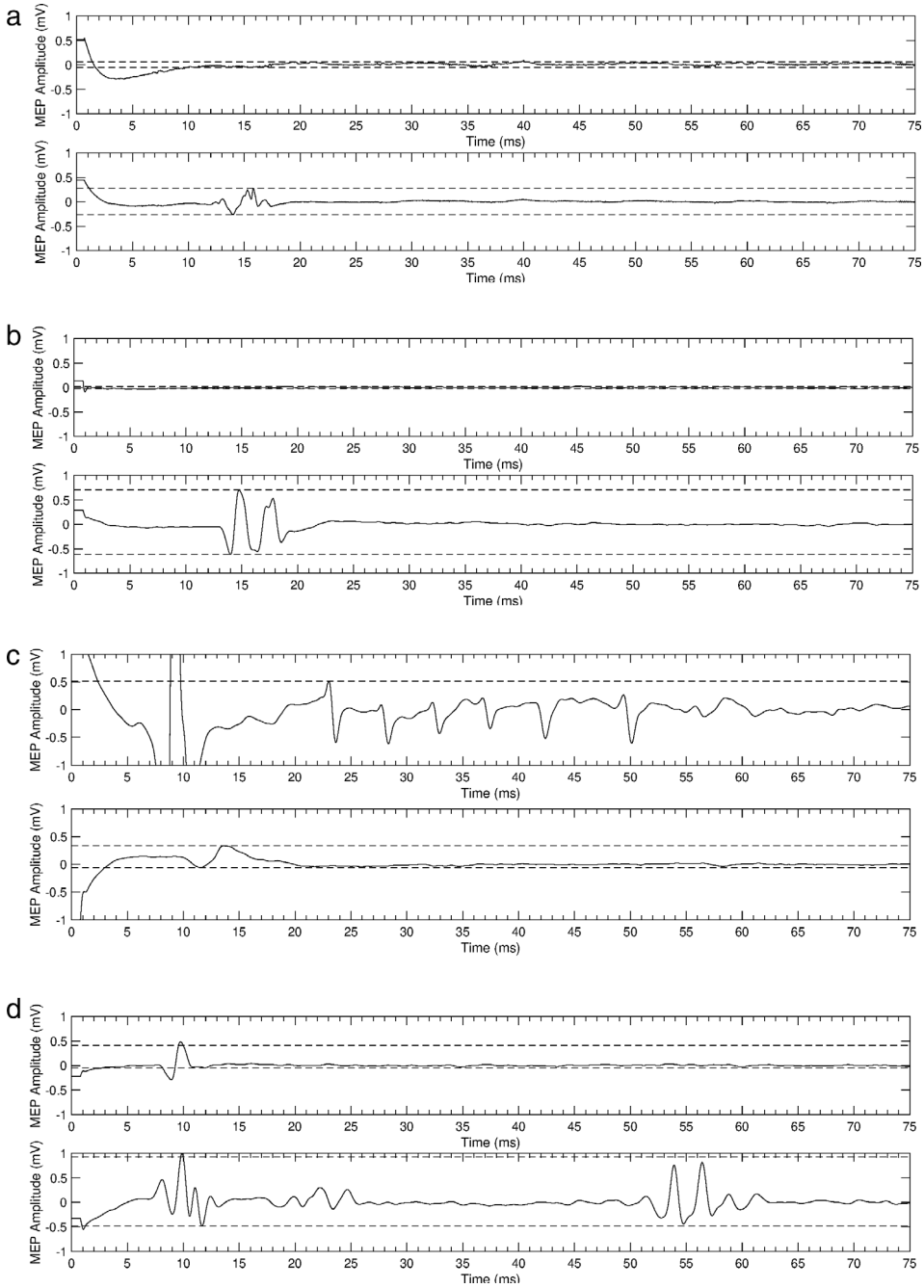

Figure 5. Representative individual electromyography (EMG) traces with TMS-induced motor evoked potentials (MEPs). EMG traces (in mV) recorded from ipsi- and contralateral forelimbs as a function of time (in ms) after unilateral TMS over the motor cortex with a small (panel a) or large (panel b) TMS coil. c, d. Spurious signals detected in EMG data when using the small TMS coil. Continued twitches are visible in the signal, which seems to be unrelated to the TMS pulse. The dotted lines indicate the minimum and maximum amplitudes of the EMG reading between 7 and 25 ms after the TMS stimulus. The difference between these two time points was taken as the MEP amplitude in mV. TMS, transcranial magnetic stimulation.

depend on the activation of different circuitries involved in the MEP response. The involvement of subcortical structures in the *in vivo* MEP response could explain the discrepancy with our simulation data, as the simulated MEPs did not take these regions into account. Furthermore, the electric field remains the most difficult feature to predict because of its dependence on a wide variety of factors, such as current intensity, coil location, head/brain anatomy, and tissue biophysics (33–35). Although computational models have proven to be useful in the guidance of stimulation protocols and to ensure target engagement (36–38), they still cannot predict the physiological outcome of noninvasive brain stimulation. This is largely due to the knowledge gap between the biophysics of stimulation, namely electric fields, and the resulting physiological effects (35).

Overall, the strong lateralization of the majority of MEPs in our study suggests that signals originated from one hemisphere. In agreement with other studies that measured cortically derived MEPs induced by direct electrical stimulation and TMS in rats, MEPs have a complex polyphasic morphology, signifying a cortical origin, with a relatively long onset latency of 7–25 ms, which is caused by the summation of excitatory post-synaptic potentials mediated by several

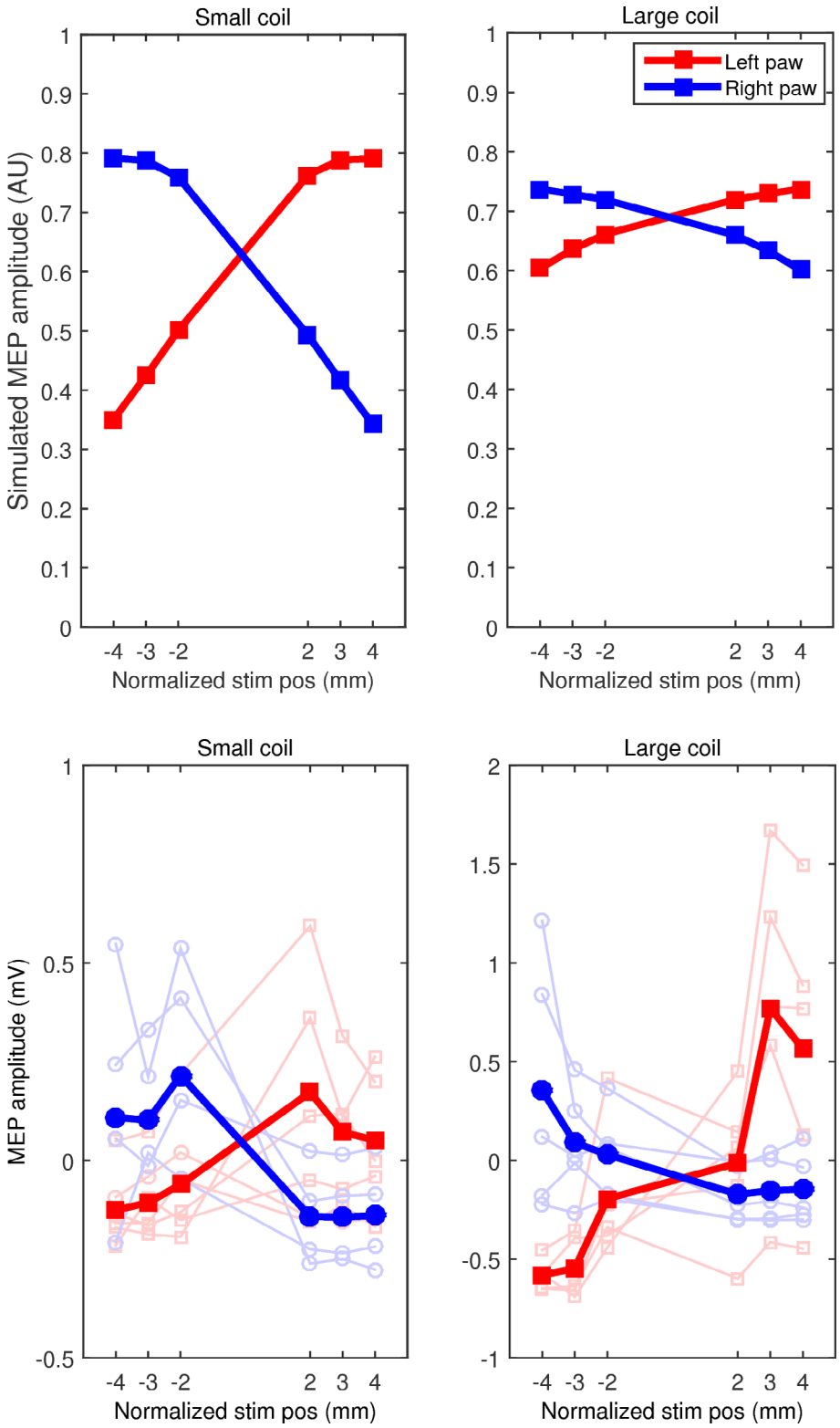

Figure 6. TMS coil laterality plots; *in silico* and *in vivo* validation. Top view: *In silico* simulations of the small coil showed a substantial difference in motor evoked potential (MEP) amplitudes when either stimulating the left (–) or right (+) hemispheres independently. This laterality was not obvious for the large coil. Details of the neuromuscular system nor the EMG needle electrodes were modeled, hence this approach does not allow absolute predictions of MEP amplitudes in terms of mV. Therefore, modeled MEP amplitudes are reflected in arbitrary units (AU). Bottom view: MEP amplitudes measured *in vivo* for the small and large TMS coils. Stimulation of one hemisphere with either the small or the large TMS coil resulted in a clear difference between the MEP responses detected in the contralateral (higher MEP amplitude) and ipsilateral forelimbs (lower MEP amplitude), respectively, indicative of TMS laterality for both coils. The horizontal axis (mm) gives the relative position of TMS at three positions in either the left (–) or right (+) hemisphere. The three stimulation positions in each hemisphere correspond to the relative motor hotspot position (–3/ 3), and positions 1 mm medial (–2/ 2) and lateral (–4/ 4) to the hotspot. The vertical axis (mV) gives the rectified MEP amplitude. The bold lines in the graphs depict the average MEP responses for five animals, while the non-bold lines represent average MEPs for each rat individually (bottom view). TMS, transcranial magnetic stimulation; pos, position. [Color figure can be viewed at wileyonlinelibrary.com]

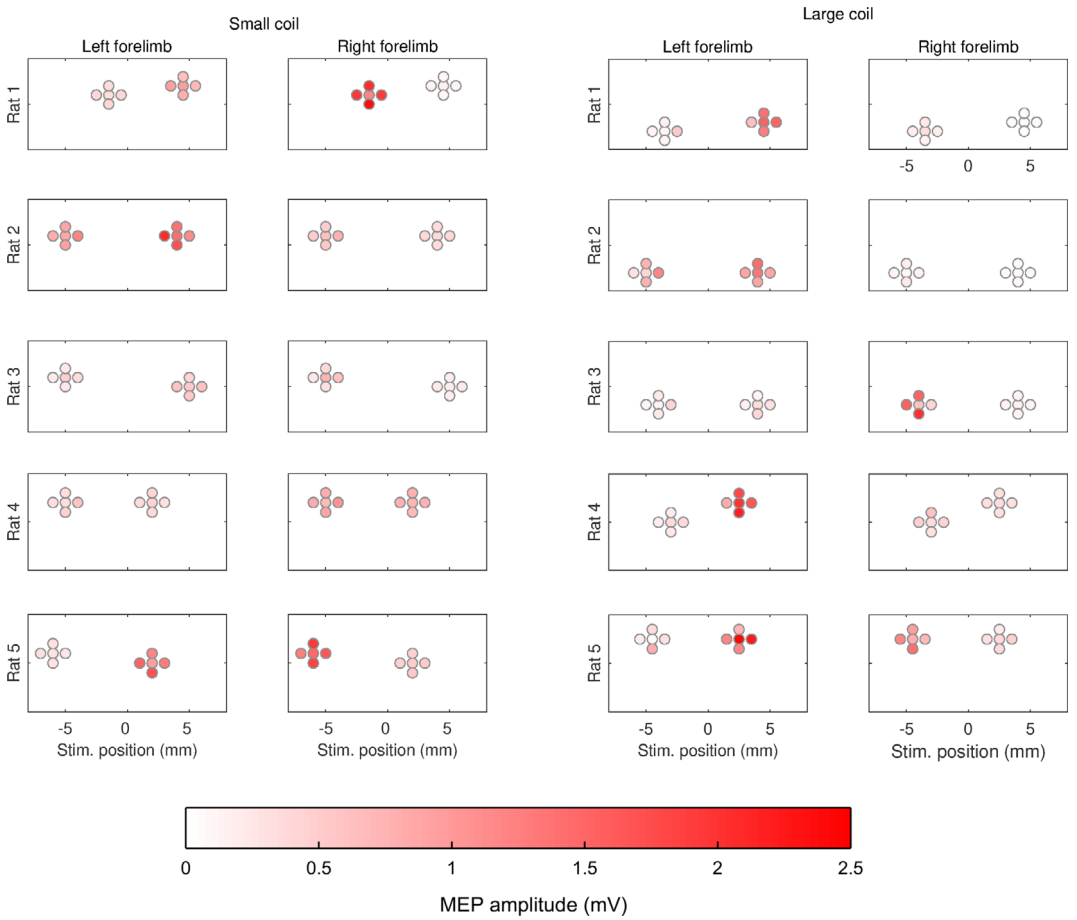

Figure 7. Five-point TMS-MEP grid map of the forelimb region of the rat motor cortex. Averaged MEP responses recorded for the left and right forelimb in five rats, using a small rodent-specific TMS coil (left) and a large commercial human TMS coil (right). Horizontal axis (mm) informs on the five-point stimulation positions in the lateral-medial (midline: 0) plane on the left (−) and right (+) hemispheres, respectively. The central grid point position was regarded as the MEP hotspot location, with the surrounding four grid-points being 1 mm anterior, medial, posterior, or lateral from the hotspot position. TMS, transcranial magnetic stimulation; MEP, motor evoked potential. [Color figure can be viewed at wileyonlinelibrary.com]

descending motor tracts (6,27,28). According to Nielsen and colleagues, the size and latency of MEPs in rats critically depend on coil position and stimulation intensity, as these parameters determine the relative contribution of differently activated motor tracts on MEP morphology. The variable MEPs observed in our study could reflect the activation of multiple descending motor tracts, including the cortico- and reticulospinal tracts, which might have contributed to MEP morphology in varying degrees. Furthermore, the observed variability in hemispheric MTs and MEP amplitudes may also be explained by differences in the contribution and number of activated motor tracts during stimulation.

MEPs elicited with the small and large coils differed considerably in amplitude and reproducibility. MEP amplitudes generated with the large coil were approximately twice as high as those elicited by the small coil. Additionally, MEP generation with the large coil seemed to be more reliable and consistent than with the small coil. Due to the dimensions of the large coil it can produce a wider electrical field spread than the small coil (39), resulting in greater neuronal recruitment responsible for producing more reproducible and larger MEPs (40). While the small coil had better focality and deeper field penetration, due to the superior power decay curve, the applied stimulation intensities might have been insufficient to excite the relevant physiological area in its entirety. Additionally, this could explain the irregular MEPs with multiple volleys/ripples, and highly variable and relatively long latencies, after the TMS pulse. Nielsen and colleagues reported similar long-latency MEPs, recorded in the biceps brachii of rats, that were elicited by weak TMS stimulus intensities just above MEP threshold (28). In addition, it is possible that the power used for the small coil was not always sufficient to elicit stable suprathreshold MEPs. Increasing the MO intensity of the small coil to elicit more stable suprathreshold MEPs would be an option. However, MO intensities above 85% poses challenges and limitations with regard to heating, particularly for rTMS protocols, even under active cooling.

Regarding translatability to human rTMS studies, our small rodent coil is able to execute typical inhibitory (e.g., 1 Hz) and facilitatory (e.g., 5 Hz) rTMS protocols and can easily apply 1200 pulses within one treatment session, granted that the MT of the rat is within an acceptable range.

Our study was limited by the superior power decay curve of the small coil, which may have caused the applied stimulation intensities (at 100% MT for each rat) to be insufficient for activation of the front limb region in its entirety to elicit reliable MEPs. TMS MEP assessment in humans (41) and animals (20) is often performed at 120–150% of the MT. Thus, stimulation with the small coil at these levels might generate more reliable MEPs. Furthermore, even though we were able to elicit lateralized MEPs in the rat motor cortex using two different coils, we did not test coil orientation effects. Salvador and Miranda have, for example, shown in a small animal TMS modeling study that the total

electric field induced by a right–left (medio-lateral) orientation of a 25 mm figure-of-eight coil has a smaller magnitude but decays more slowly than the field induced by a posterior–anterior orientation (30). The posterior–anterior orientation of the TMS coils in our study could have further contributed to the observed MEP variability.

CONCLUSIONS

In this study we have combined *in vivo* and *in silico* experiments to guide the design of an optimal small rodent TMS coil capable of inducing a strong enough electric field in relatively confined cortical regions. *In silico* simulations suggested favorable ability of this coil in comparison to larger commercially available human coils. Our *in vivo* data showed that MEP asymmetry can be achieved with the novel TMS coil, although this was also feasible with a larger conventional TMS coil. Our study demonstrates that focal TMS stimulation can be accomplished in translational rodent studies. The apparent discrepancy between our *in silico* and *in vivo* results is an important consideration for follow-up studies.

Acknowledgements

This work was supported by the Netherlands Organization for Scientific Research [VICI 016.130.662] and by the DeNeCor project being part of the ENIAC Joint Undertaking. Both funding sources had no further role in the study design or in the collection, analysis, and interpretation of the data. The authors would like to thank Gerard van Vliet, Ivan Loginov and Anna Maslyukova for their technical assistance.

Authorship Statements

Julia Boonzaier, Petar Petrov, Sebastiaan F. W. Neggers and Rick M. Dijkhuizen designed the study. Julia Boonzaier and Petar Petrov performed literature searches and wrote the manuscript. Julia Boonzaier performed motor threshold and motor evoked potential measurements. Petar Petrov constructed the 3D rat brain model and performed computer simulations. Willem M. Otte acquired and segmented the high-resolution MRI data used to construct the 3D rat brain model and assisted with the manuscript preparation. Sebastiaan F. W. Neggers processed the EMG data and performed the data analysis. Nickolay Smirnov provided technical assistance on the use of the Neurosoft equipment and assisted with the proofreading of the manuscript together with Sebastiaan F. W. Neggers and Rick M. Dijkhuizen. All authors have contributed to and have approved the final manuscript.

How to Cite this Article:

Boonzaier J., Petrov P.I., Otte W.M., Smirnov N., Neggers S. F.W., Dijkhuizen R.M. 2020. Design and Evaluation of a Rodent-Specific Transcranial Magnetic Stimulation Coil: An *In Silico* and *In Vivo* Validation Study. Neuromodulation 2020; 23: 324–334

REFERENCES

1. Dayan E, Censor N, Buch ER, Sandrini M, Cohen LG. Noninvasive brain stimulation: from physiology to network dynamics and back. *Nat Neurosci* 2013;16: 838–844. https://doi.org/10.1038/nn.3422.
2. Lefaucheur J-P, André-Obadia N, Antal A et al. Evidence-based guidelines on the therapeutic use of repetitive transcranial magnetic stimulation (rTMS). *Clin Neurophysiol* 2014;125:2150–2206. https://doi.org/10.1016/j.clinph.2014.05.021.
3. Tang A, Thickbroom G, Rodger J. Repetitive transcranial magnetic stimulation of the brain: mechanisms from animal and experimental models. *Neuroscientist* 2017;23:82–94. https://doi.org/10.1177/1073858415618897.
4. Tang AD, Lowe AS, Garrett AR et al. Construction and evaluation of rodent-specific rTMS coils. *Front Neural Circuits* 2016;10:1–10. https://doi.org/10.3389/fncir.2016.00047.
5. Vahabzadeh-Hagh AM, Muller PA, Gersner R, Zangen A, Rotenberg A. Translational neuromodulation: approximating human transcranial magnetic stimulation protocols in rats. *Neuromodulation.* 2012;15:296–305. https://doi.org/10.1111/j.1525-1403.2012.00482.x.
6. Rotenberg A, Muller PA, Vahabzadeh-Hagh AM et al. Lateralization of forelimb motor evoked potentials by transcranial magnetic stimulation in rats. *Clin Neurophysiol* 2010;121:104–108. https://doi.org/10.1016/j.clinph.2009.09.008.
7. Cohen D, Cuffin BN. Developing a more focal magnetic stimulator. Part I: some basic principles. *J Clin Neurophysiol* 1991;8:102–111. https://doi.org/10.1097/00004691-199101000-00013.
8. Parthoens J, Verhaeghe J, Servaes S, Miranda A, Stroobants S, Staelens S. Performance characterization of an actively cooled repetitive transcranial magnetic stimulation coil for the rat. *Neuromodulation.* 2016;19:459–468. https://doi.org/10.1111/ner.12387.
9. Rodger J, Mo C, Wilks T, Dunlop SA, Sherrard RM. Transcranial pulsed magnetic field stimulation facilitates reorganization of abnormal neural circuits and corrects behavioral deficits without disrupting normal connectivity. *FASEB J* 2012;26: 1593–1606. https://doi.org/10.1096/fj.11-194878.
10. Makowiecki K, Harvey AR, Sherrard RM, Rodger J. Low-intensity repetitive transcranial magnetic stimulation improves abnormal visual cortical circuit topography and upregulates BDNF in mice. *J Neurosci* 2014;34:10780–10792. https://doi.org/10.1523/JNEUROSCI.0723-14.2014.
11. Grehl S, Viola HM, Fuller-Carter PI et al. Cellular and molecular changes to cortical neurons following low intensity repetitive magnetic stimulation at different frequencies. *Brain Stimul* 2015;8:114–123. https://doi.org/10.1016/j.brs.2014.09.012.
12. Meng Q, Jing L, Badjo JP et al. A novel transcranial magnetic stimulator for focal stimulation of rodent brain. *Brain Stimul* 2018;11:663–665. https://doi.org/10.1016/j.brs.2018.02.018.
13. Petrov PI, Mandija S, Sommer IEC, Van Den Berg CAT, Neggers SFW. How much detail is needed in modeling a transcranial magnetic stimulation figure-8 coil: measurements and brain simulations. *PLoS One* 2017;12:e0178952. https://doi.org/10.1371/journal.pone.0178952.
14. Otte WM, Dijkhuizen RM. Rat brain template. Open Science Framework. https://osf.io/epy5d/. Accessed April 6, 2018.
15. Bronson JR, Sastry SP, Levine JA, Whitaker RT. Adaptive and unstructured mesh cleaving. *Procedia Eng* 2014;82:266–278. https://doi.org/10.1016/j.proeng.2014.10.389.
16. Wagner TA, Zahn M, Grodzinsky AJ, Pascual-Leone A. Three-dimensional head model simulation of transcranial magnetic stimulation. *IEEE Trans Biomed Eng* 2004;51:1586–1598. https://doi.org/10.1109/TBME.2004.827925.
17. Opitz A, Windhoff M, Heidemann RM, Turner R, Thielscher A. How the brain tissue shapes the electric field induced by transcranial magnetic stimulation. *Neuroimage* 2011;58:849–859. https://doi.org/10.1016/j.neuroimage.2011.06.069.
18. Fonoff ET, Pereira JF, Camargo LV et al. Functional mapping of the motor cortex of the rat using transdural electrical stimulation. *Behav Brain Res* 2009;202: 138–141. https://doi.org/10.1016/j.bbr.2009.03.018.
19. Whishaw IQ, Cioe JDD, Previsich N, Kolb B. The variability of the interaural line vs the stability of bregma in rat stereotaxic surgery. *Physiol Behav* 1977;19:719–722. https://doi.org/10.1016/0031-9384(77)90304-3.
20. Luft A, Kaelin-Lang A, Hauser T-K, Cohen L, Thakor N, Hanley D. Transcranial magnetic stimulation in the rat. *Exp Brain Res* 2001;140:112–121. https://doi.org/10.1007/s002210100805.
21. Haghighi SS, Madsen R, Green KD, Oro JJ, Kracke GR. Suppression of motor evoked potentials by inhalation anesthetics. *J Neurosurg Anesthesiol* 1990;2: 73–78. http://www.ncbi.nlm.nih.gov/pubmed/15815324.
22. Haghighi SS, Green KD, Oro JJ, Drake RK, Kracke GR. Depressive effect of isoflurane anesthesia on motor evoked potentials. *Neurosurgery* 1990;26:993–997.
23. Wiechers DO, Blood JR. EMG needle electrodes: electrical impedance. *Arch Phys Med Rehabil* 1979;60:364–369. http://www.ncbi.nlm.nih.gov/pubmed/464781 Accessed November 28, 2017.
24. Rossini P, Barker A, Berardelli A et al. Non-invasive electrical and magnetic stimulation of the brain, spinal cord and roots: basic principles and procedures for routine clinical application. Report of an IFCN committee. *Electroencephalogr Clin Neurophysiol* 1994;91:79–92. https://doi.org/10.1016/0013-4694(94)90029-9.
25. Vaseghi B, Zoghi M, Jaberzadeh S. Inter-pulse interval affects the size of single-pulse TMS-induced motor evoked potentials: a reliability study. *Basic Clin Neurosci* 2015;6:44–51. https://www.ncbi.nlm.nih.gov/pmc/articles/PMC4741267/pdf/BCN-6-44.pdf Accessed November 29, 2017.
26. Thomson RH, Maller JJ, Daskalakis ZJ, Fitzgerald PB. Blood oxygenation changes resulting from trains of low frequency transcranial magnetic stimulation. *Cortex* 2012;48:487–491. https://doi.org/10.1016/j.cortex.2011.04.028.

27. Schlag MG, Hopf R, Redl H. Serial recording of sensory, corticomotor, and brainstem-derived motor evoked potentials in the rat. *Somatosens Mot Res* 2001; 18:106–116. https://doi.org/10.1080/13557850101200621 9.
28. Nielsen JB, Perez MA, Oudega M, Enriquez-Denton M, Aimonetti JM. Evaluation of transcranial magnetic stimulation for investigating transmission in descending motor tracts in the rat. *Eur J Neurosci* 2007;25:805–814. https://doi.org/10.1111/j.1460-9568.2007.05326.x.
29. Chang WH, Fried PJ, Saxena S et al. Optimal number of pulses as outcome measures of neuronavigated transcranial magnetic stimulation. *Clin Neurophysiol* 2016;127:2892–2897. https://doi.org/10.1016/j.clinph.2016.04.001.
30. Salvador R, Miranda PC. Transcranial magnetic stimulation of small animals: a modeling study of the influence of coil geometry, size and orientation. *Conf Proc IEEE Eng Med Biol Soc* 2009;2009:674–677. https://doi.org/10.1109/IEMBS.2009.5334070.
31. Weissman JD, Epstein CM, Davey KR. Magnetic brain stimulation and brain size: relevance to animal studies. *Electroencephalogr Clin Neurophysiol Potentials Sect* 1992;85:215–219. https://doi.org/10.1016/0168-5597(92)90135-X.
32. Vahabzadeh-Hagh AM, Muller PA, Pascual-Leone A, Jensen FE, Rotenberg A. Measures of cortical inhibition by paired-pulse transcranial magnetic stimulation in anesthetized rats. *J Neurophysiol* 2010;105:615–624. https://doi.org/10.1152/jn.00660.2010.
33. Miranda PC, Mekonnen A, Salvador R, Ruffini G. The electric field in the cortex during transcranial current stimulation. *Neuroimage* 2013;70:48–58. https://doi.org/10.1016/j.neuroimage.2012.12.034.
34. Opitz A, Paulus W, Will S, Antunes A, Thielscher A. Determinants of the electric field during transcranial direct current stimulation. *Neuroimage* 2015;109:140–150. https://doi.org/10.1016/j.neuroimage.2015.01.033.
35. Alekseichuk I, Mantell K, Shirinpour S, Opitz A. Comparative modeling of transcranial magnetic and electric stimulation in mouse, monkey, and human. *Neuroimage* 2019;194:136–148. https://doi.org/10.1101/442426.
36. Huang Y, Liu AA, Lafon B et al. Measurements and models of electric fields in the *in vivo* human brain during transcranial electric stimulation. *Elife* 2017;6:1–26. https://doi.org/10.7554/elife.18834.
37. Opitz A, Falchier A, Yan C-G et al. Spatiotemporal structure of intracranial electric fields induced by transcranial electric stimulation in humans and nonhuman primates. *Sci Rep* 2016;6:31236. https://doi.org/10.1038/srep31236.
38. Opitz A, Yeagle E, Thielscher A, Schroeder C, Mehta AD, Milham MP. On the importance of precise electrode placement for targeted transcranial electric stimulation. *Neuroimage* 2018;181:560–567. https://doi.org/10.1016/j.neuroimage.2018.07.027.
39. De DZ, Lisanby SH, Peterchev AV. Electric field depth-focality tradeoff in transcranial magnetic stimulation: simulation comparison of 50 coil designs. *Brain Stimul* 2013;6:1–13. https://doi.org/10.1016/j.brs.2012.02.005.
40. Cortes M, Black-Schaffer RM, Edwards DJ. Transcranial magnetic stimulation as an investigative tool for motor dysfunction and recovery in stroke: an overview for neurorehabilitation clinicians. *Neuromodulation* 2012;15:319–325. https://doi.org/10.1111/j.1525-1403.2012.00459.x.
41. Vink JJT, Petrov PI, Mandija S, Dijkhuizen RM, Neggers SFW. Outcome of TMS-based motor mapping depends on TMS current direction. *bioRxiv* 2018;371997. https://doi.org/10.1101/371997.

SUPPORTING INFORMATION

Additional supporting information may be found online in the supporting information tab for this article.

